SOURCE DATA   TRANSPARENT PROCESS

THE EMBO JOURNAL

The *Arabidopsis* ALF4 protein is a regulator of SCF E3 ligases

Rammyani Bagchi[1], Charles W Melnyk[2,†] (iD), Gideon Christ[3], Martin Winkler[3,4], Kerstin Kirchsteiner[1], Mohammad Salehin[1], Julia Mergner[5,‡], Michael Niemeyer[3], Claus Schwechheimer[5], Luz Irina A Calderón Villalobos[3] & Mark Estelle[1,*] (iD)

Abstract

The cullin-RING E3 ligases (CRLs) regulate diverse cellular processes in all eukaryotes. CRL activity is controlled by several proteins or protein complexes, including NEDD8, CAND1, and the CSN. Recently, a mammalian protein called Glomulin (GLMN) was shown to inhibit CRLs by binding to the RING BOX (RBX1) subunit and preventing binding to the ubiquitin-conjugating enzyme. Here, we show that *Arabidopsis* ABERRANT LATERAL ROOT FORMATION4 (ALF4) is an ortholog of GLMN. The *alf4* mutant exhibits a phenotype that suggests defects in plant hormone response. We show that ALF4 binds to RBX1 and inhibits the activity of SCF^{TIR1}, an E3 ligase responsible for degradation of the Aux/IAA transcriptional repressors. *In vivo*, the *alf4* mutation destabilizes the CUL1 subunit of the SCF. Reduced CUL1 levels are associated with increased levels of the Aux/IAA proteins as well as the DELLA repressors, substrate of SCF^{SLY1}. We propose that the *alf4* phenotype is partly due to increased levels of the Aux/IAA and DELLA proteins.

Introduction

Ubiquitin–protein conjugation is a highly regulated process that involves ubiquitin-activating and conjugating enzymes (E1 and E2), as well as a ubiquitin ligase (E3). The E3 ligase coordinates with the E2 enzyme to conjugate ubiquitin to lysine residues in the substrate protein. The cullin-RING ligases (CRLs) are a large class of E3 ligases that consist of a cullin, a RING protein called RING BOX 1 (RBX1), and a substrate adapter protein (Hua & Vierstra, 2011). In humans, CRLs have been implicated in a wide variety of cellular processes, including those related to cancer, while in plants they have a central role in diverse developmental and physiological processes (Hua & Vierstra, 2011; Kelley & Estelle, 2012; Zheng *et al*, 2016). The Skp1-Cullin1-F-box (SCF) E3s are a subclass of CRLs in which the substrate adapter consists of Skp1 (ASK in plants) and an F-box protein. Although there are many F-box proteins in all eukaryotes, the family has dramatically expanded in plants (~700 in *Arabidopsis*), suggesting that SCFs have been co-opted for many cellular and developmental programs (Gagne *et al*, 2002).

SCF regulation is a highly dynamic process that involves several proteins and protein complexes (Deshaies & Joazeiro, 2009; Hua & Vierstra, 2011; Lydeard *et al*, 2013). These E3s are activated by conjugation of the ubiquitin-related protein RELATED TO UBIQUITIN (RUB), or NEDD8 in animals, to the C-terminus of the cullin subunit. Neddylation causes dramatic conformational changes in CUL1 and RBX1 that allow the RING domain on RBX1 to interact with the E2 (Duda *et al*, 2008). On the other hand, SCFs are inhibited by the COP9 SIGNALOSOME (CSN) through its de-neddylating activity as well as by direct binding to the SCF (Enchev *et al*, 2012). Another protein, CULLIN-ASSOCIATED NEDD8-DISSOCIATED PROTEIN 1 (CAND1), binds to the cullin and is important for substrate adapter exchange (Pierce *et al*, 2013; Wu *et al*, 2013; Zemla *et al*, 2013).

The human disease glomuvenous malformation, characterized by cutaneous lesions, is caused by mutations in the *Glomulin* (*GLMN*) gene. In the familial form of this disease, affected individuals typically carry one loss-of-function *glmn* allele and experience a second somatic *glmn* mutation in the affected tissue (Duda *et al*, 2012; Tron *et al*, 2012). The *glmn* null mice die as embryos, suggesting that the gene is probably essential in humans (Tron *et al*, 2012). Recent studies indicate that GLMN regulates CRLs by binding to RBX1 and preventing the E2-conjugating enzyme from engaging the CRL (Duda *et al*, 2012; Tron *et al*, 2012). In human cells, one

1 Howard Hughes Medical Institute, University of California San Diego, La Jolla, CA, USA
2 Sainsbury Laboratory, University of Cambridge, Cambridge, UK
3 Department of Molecular Signal Processing, Leibniz Institute of Plant Biochemistry, Halle, Germany
4 Institute of Biology, Structural Biology/Biochemistry, Humboldt-University Berlin, Berlin, Germany
5 Plant Systems Biology, Technische Universität München, Freising, Germany
   *Corresponding author. Tel: +1 858 246 0453; E-mail: mestelle@ucsd.edu
   †Present address: Department of Plant Biology, Swedish University of Agricultural Sciences, Uppsala, Sweden
   ‡Present address: Proteomics and Bioanalytics, Technische Universität München, Freising, Germany

known consequence of *glmn* mutations is a decrease in the amount of the F-box protein Fbw7 and an increase in the level of Fbw7 substrates cyclin E and c-Myc (Tron *et al*, 2012).

There are several well-characterized SCFs in plants, including SCF[TIR1] and SCF[SLY1] (Schwechheimer & Willige, 2009; Salehin *et al*, 2015; Lavy & Estelle, 2016). SCF[TIR1] promotes the degradation of transcriptional repressors called Aux/IAA proteins in response to the hormone auxin, while SCF[SLY1] promotes degradation of another class of transcriptional regulators, the DELLA proteins, in response to the hormone gibberellic acid (GA). Strikingly, several SCF subunits, as well as regulators of SCF activity, were originally identified through screens for auxin-resistant mutants in *Arabidopsis* (Walker & Estelle, 1998).

The *Arabidopsis aberrant lateral root formation 4* (*alf4*) mutant exhibits a number of auxin-related defects but its role in auxin signaling is unknown. The mutant was isolated in a screen for defects in root architecture, particularly a dramatic reduction in lateral root formation (Celenza *et al*, 1995; DiDonato *et al*, 2004). In addition, *ALF4* is required for protoplast regeneration, callus formation, and efficient graft formation (Chupeau *et al*, 2013; Melnyk *et al*, 2015; Shang *et al*, 2016). Here, we demonstrate that ALF4 inhibits SCF ligases and is related to mammalian GLMN. Further, we show that Aux/IAA and DELLA proteins accumulate in the *alf4* mutant. These results suggest that the developmental defects ascribed to the mutant are at least partly due to defects in hormone signaling.

Results

The *alf4* mutants are resistant to auxin and display defects in root and shoot growth

Previous studies established that the *alf4-1* mutant has a normal primary root, but is deficient in lateral root initiation (Celenza *et al*, 1995; DiDonato *et al*, 2004). We confirmed this phenotype with three *alf4* alleles containing deletions or T-DNA insertions (Figs 1A and B, and EV1). All three lines had normal or near-normal primary root elongation but formed dramatically fewer lateral roots. In addition, all three alleles were affected in shoot development (Fig 1C and D). The rosettes of mutant plants were much smaller than the wild-type control and had distorted leaves and twisted petioles. Rarely did the *alf4-2* or *alf4-063* mutants survive long enough to flower on soil, but *alf4-1* produced a short and largely infertile

inflorescence. Based on these results and previous observations, it is likely that *alf4-1*, a 12-bp deletion mutant, is not a null allele (DiDonato *et al*, 2004). To determine whether the effect of the mutation on the shoot was due to a reduced root system, we grafted *alf4* scions onto Col-0 wild-type root stocks. As shown in Fig 1C and D, the wild-type root stock enhanced growth of the mutant shoot and increased fertility of the *alf4-1* shoot. However, scions from *alf4-2* and *alf4-063* remained severely affected, indicating that ALF4 function was required in the shoot.

The phenotype of the *alf4* mutant suggests a defect in auxin signaling. To address this possibility, we examined the effects of auxin on primary root growth in *alf4-1* and Col-0 plants and found that the mutant was resistant to low concentrations of IAA (Fig 1E). Further, *alf4-1* plants exhibited a delayed gravitropic response, consistent with a defect in auxin signaling (Fig 1F). To determine whether ALF4 was required for the transcriptional response to auxin, we introduced the *pDR5:GFP* reporter into the *alf4*-1 mutant. We found that GFP signal was reduced in the mutant compared to the wild type in the absence and presence of the auxin 1-naphthyl acetic acid (NAA) (Fig 1G and H). In contrast, the response to the cytokinin N6-benzyladenine (BA) using the *pARR5:GFP* cytokinin reporter was largely unaffected in the *alf4* mutant (Fig EV2). These results suggest that the pleiotropic phenotype exhibited by the *alf4* mutants may be partly due to reduced auxin response.

Expression of ALF4 in the root

The *ALF4* gene is broadly expressed throughout the plant (DiDonato *et al*, 2004). To further examine expression of *ALF4* in the root, we analyzed the previously published *pALF4:ALF4-GFP* line (DiDonato *et al*, 2004). We found that ALF4 protein was present in the nuclei of cells in the primary root tip, particularly the epidermal cells, and in the vascular tissue (Fig 2A and F). Consistent with the lateral root defect, ALF4 protein begins to accumulate in the lateral root primordium and continues to increase in levels throughout formation of the lateral root meristem and emergence of the lateral root (Fig 2B–E). To determine whether the *ALF4* gene was regulated by auxin or cytokinin, we also treated the *pALF4:ALF4-GFP* line with NAA, the auxin transport inhibitor naphthylphthalamic acid (NPA), and BA. We did not observe a clear effect of these treatments on expression of the transgene (Fig EV2). In addition, publically available data show that *ALF4* is not regulated by GA (http://bar.utoronto.ca) (Winter *et al*, 2007).

Figure 1. The *alf4* mutants exhibit a pleiotropic phenotype.

A, B Primary root length (A) and lateral root number (B) of wild-type and mutant seedlings (different letters represent significant differences within a time point, mean ± SE, n = 34–49 roots/treatment, ANOVA with Tukey's *post hoc* test, $P < 0.01$).

C Wild-type and mutant plants 35 days after grafting. The top row are ungrafted, while the bottom row are mutant scion grafted onto a Col-0 root stock.

D Wild-type and mutant plants 70 days after grafting.

E Effect of auxin on wild-type and *alf4-1* root growth. Five-day-old seedlings were transferred to fresh medium ± IAA and allowed to grow for 3 days. Growth is presented as the percentage of the DMSO control treatment for each genotype. Each value represents the mean, and error bars represent standard deviation ($n \geq 10$).

F Gravitropic response in wild-type and *alf4-1* seedlings. Seedlings grown on agar medium were rotated 90 degrees at t = 0. The angle of curvature from the horizontal was measured at the times indicated. Each point represents the mean of six measurements. Error bars represent the standard deviation ($n \geq 10$).

G Expression of the auxin-responsive marker, *pDR5:GFP*, (green signal) imaged in the presence or absence of synthetic auxin NAA for 24 h. Roots were counterstained with propidium iodide (red signal).

H Quantification of GFP in (G) (different letters represent significant differences between groups, mean ± SE, n = 9–15 root tips/treatment, ANOVA with Tukey's *post hoc* test, $P < 0.01$).
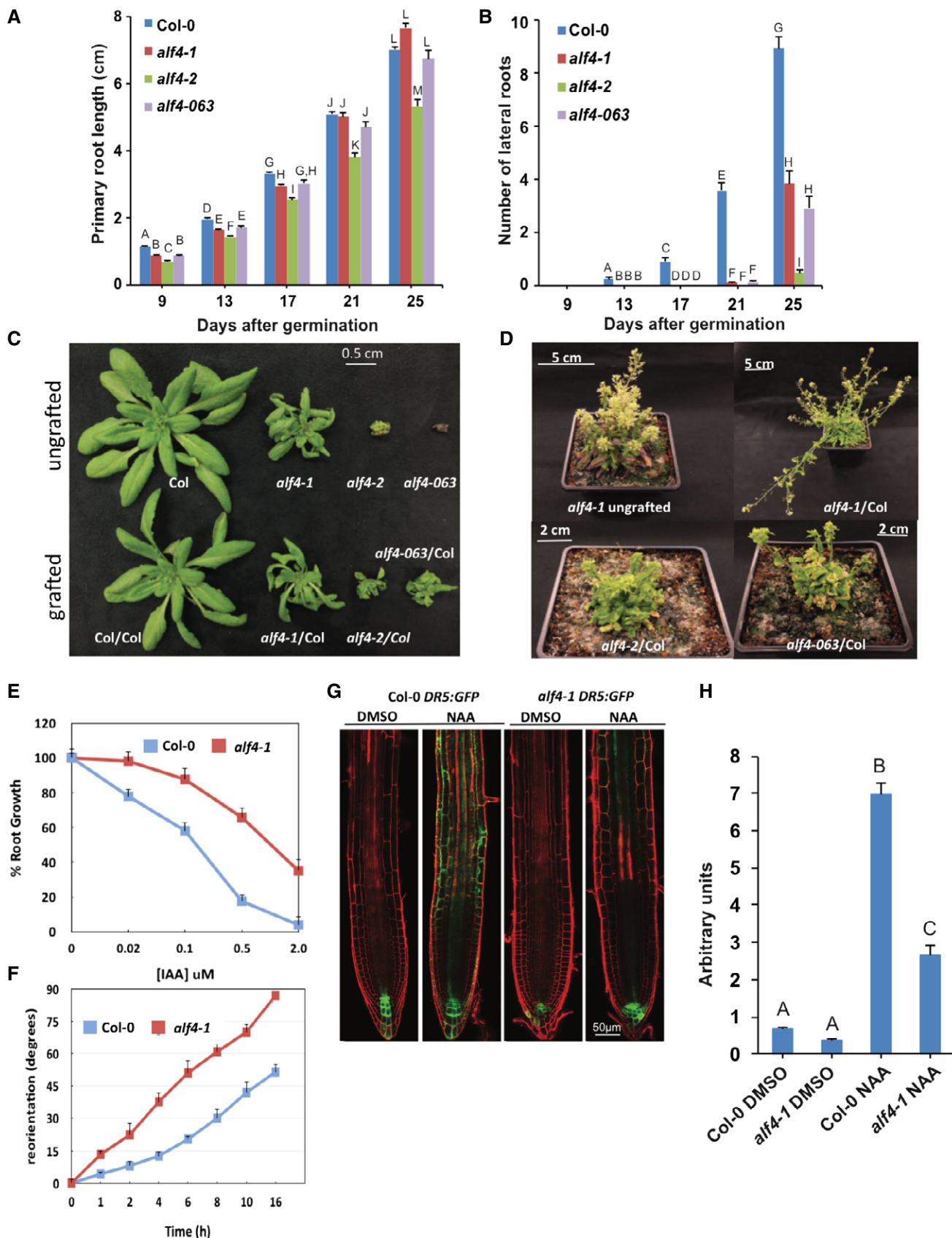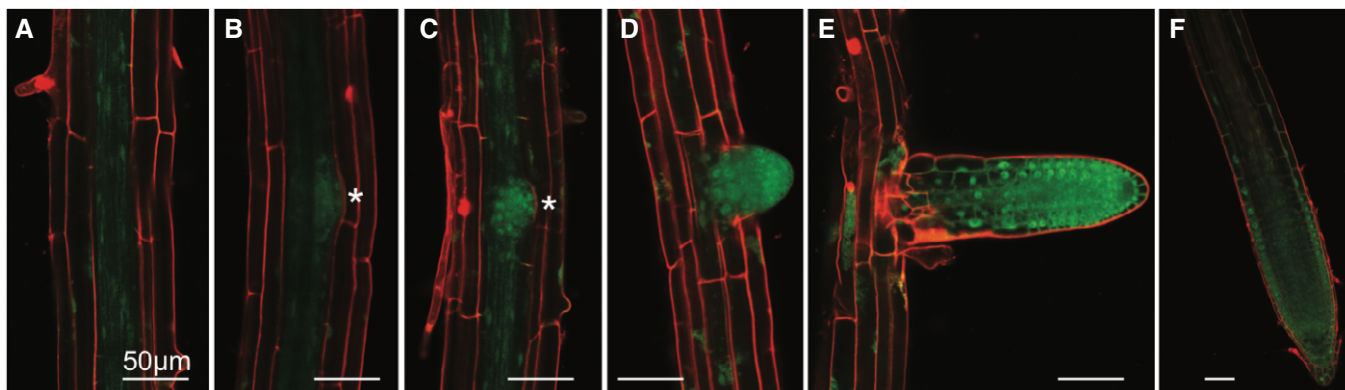
Figure 1.

Figure 2. ALF4 protein accumulates during lateral root formation.

pALF4:ALF4-GFP seedlings display ALF4-GFP (green signal) and are counterstained with propidium iodide (red signal). Scale bar is 50 μm.

A   *ALF4* is expressed in the vasculature.

B–E ALF4 protein accumulates in the lateral root primordium and the emerging lateral root. Asterisks highlight the location of the emerging lateral root.

F   ALF4 protein is also present throughout the primary root tip.

The ALF4 protein is related to GLMN and interacts with RBX1

The GLMN protein was recently shown to be an important regulator of cullin-RING E3 ligases in mammals (Duda *et al*, 2012; Tron *et al*, 2012). GLMN interacts with RBX1 and prevents binding of the E2 protein. Structural studies showed that GLMN consists of a series of helical repeats similar to HEAT repeats (Duda *et al*, 2012). The protein has two such domains, bisected by a single helix that is perpendicular to the other helices, while the RBX1-binding domain is in the C-terminal HEAT repeat domain. An amino acid alignment of GLMN and ALF4 revealed that the two proteins are ~25% identical along their entire length. Importantly, several key residues known to contribute to the interaction between GLMN and RBX1 are conserved in ALF4 (Fig EV3). In addition, the Phyre2 protein structure prediction server predicted that ALF4 was a helical repeat protein with an overall organization that is very similar to GLMN (Fig EV4) (Kelley *et al*, 2015).

To determine whether ALF4 interacted with *Arabidopsis* RBX1, we performed a series of *in vitro* and *in vivo* experiments. Yeast two-hybrid assays demonstrated a strong interaction between the two proteins in this assay (Fig 3A). To further assess this interaction, we generated two ALF4 protein variants where the conserved K484 and R614 amino acids were replaced with alanine. Both residues contribute to the interaction between GLMN and RBX1 (Duda *et al*, 2012). In addition, we generated a mutant lacking the C-terminal 94 amino acids (ALF4$^{1-532stop}$). In the yeast assay, the strength of the interaction between ALF4^{A484A614} and RBX1 was similar to that of wild-type ALF4. In contrast, ALF4$^{1-532stop}$ did not interact with RBX1, indicating that the C-terminal region of ALF4 is, as in the case of GLMN, important for RBX1 binding (Fig 3A).

To confirm the interaction between ALF4 and RBX1, we performed a co-immunoprecipitation experiment using the *pALF4:ALF4-GFP* line and an antibody directed against a peptide from human RBX1 that recognizes *Arabidopsis* RBX1 (Xu *et al*, 2002; Gilkerson *et al*, 2009). The results in Fig 3B show that RBX1 is recovered in an immunoprecipitation of ALF4-GFP, indicating that these two proteins are interacting in the plant extract. We extended

this finding using an *in vitro* pulldown experiment. As expected, wild-type ALF4 clearly interacted with RBX1 *in vitro*. However, neither ALF4^{A484A614} nor ALF4$^{1-532stop}$ were recovered in this GST-RBX1 pulldown assay, confirming that K484 and R614 are important for RBX1 binding (Fig 3C).

To demonstrate an interaction *in vivo,* we performed a BiFC (bimolecular fluorescence complementation) experiment using RBX1 with wild-type and mutant ALF4. Similar to the yeast two-hybrid and pulldown experiments, only the wild-type ALF4 protein displayed a robust interaction with RBX1 (Fig 3D). The mutant variants interacted weakly (ALF4^{A484A614}) or not at all (ALF4$^{1-532stop}$).

Finally, to quantify ALF4–RBX1 interaction when RBX1 is associated with cullin in solution, we carried out microscale thermophoresis (MST) (Fig 3E). For this experiment, recombinant, purified MmRBX1–HsCUL1 (Li *et al*, 2005) was fluorescently labeled and incubated with ALF4 at a range of concentrations. We used the mouse RBX1 and human CUL1 proteins for this experiment because their expression had been optimized (Li *et al*, 2005). Within the concentration range 7 μM to 0.21 nM, ALF4 exhibited an affinity for MmRBX1–HsCUL1 with a K_d of 346.04 ± 77.05 nM (Figs EV5 and EV6). ALF4 clearly interacted with Cul1–RBX1, and given their structural similarities, the ALF4–RBX1 interaction likely resembles that of GLMN-RBX1.

The *alf4* mutant stabilizes the SCF^{TIR1} and SCF^{SLY} substrates IAA17 and RGA

Since ALF4 may regulate CRL assembly or activity, we examined the levels of SCF^{TIR1} and SCF^{SLY1} substrates, the Aux/IAA and DELLA repressors of the auxin and gibberellin pathways, respectively. To determine the effects of *alf4* on DELLA proteins, we examined the turnover of the DELLA protein REPRESSOR OF GA1-3 (RGA) in the wild type and *alf4-063* mutant after inhibition of protein biosynthesis with cycloheximide (CHX). Immunoblots showed that RGA strongly accumulated in the *alf4* background (Fig 4A). In addition, RGA levels in *alf4* plants were not reduced
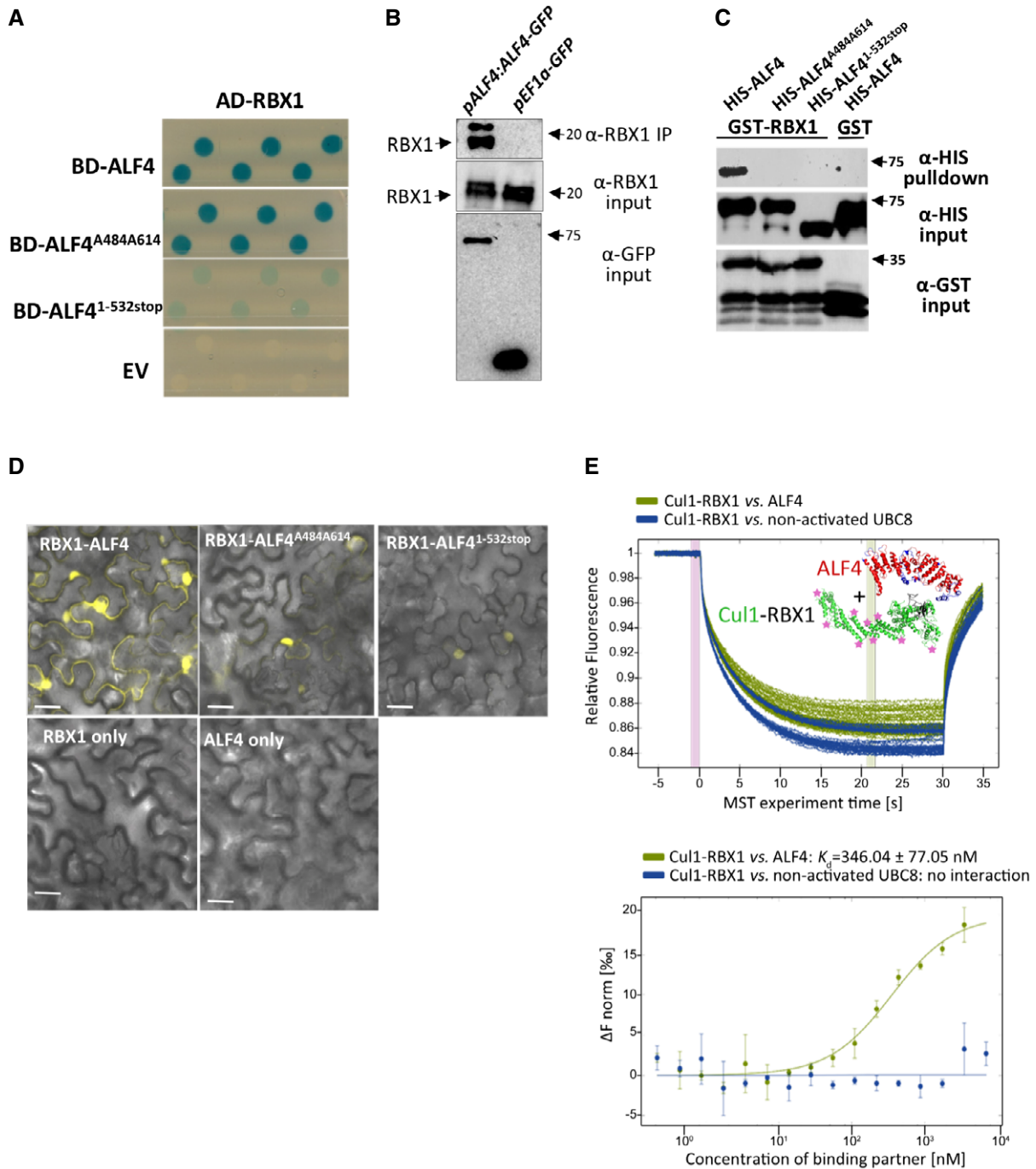
Figure 3. ALF4 interacts with RBX1.

A The ALF4$^{1\text{-}532stop}$ mutant displays reduced interaction with RBX1 in comparison with full-length ALF4 protein in a yeast two-hybrid assay. Blue color represents X-GAL staining. EV, empty vector.

B RBX1 co-immunoprecipitates with ALF4 in extracts prepared from 14-day-old *pALF4:ALF4-GFP* plants. The *pEF1a-GFP* line serves as a control.

C *In vitro* pulldown of HIS-ALF4 and ALF4 mutants with GST-tagged RBX1 or GST alone. ALF4 variants do not interact with RBX1.

D BIFC assay testing the interaction of ALF4 or ALF4 mutants in pCYCE(R) vector with RBX1 cloned in pVYNE(R). Scale bars are 50 µm.

E Microscale thermophoresis (MST) analysis of ALF4 binding to Cul1–RBX. Thermophoresis curves for protein binding over a temperature gradient and over time (upper panel), and fitted curves plotting normalized fluorescence against concentration of ligands (lower panel). HsCul1–RBX1 interacts with ALF4 with a $K_d = 346.04 \pm 77.05$ nM. Measurements were performed with a dilution series of ALF4 concentrations from 7 µM to 0.21 nM, and constant levels of fluorescently labeled Cul1–RBX1 (10 nM). Dissociation constant was calculated from three independent biological replicates. Binding of Cul1–RBX1 to not-charged E2 (UBC8) (without ubiquitin) serves as a negative control (blue). In the upper panel start (0 s) and end (21 s) of the temperature gradient were indicated with pink and green boxes, respectively. Error bars to correspond s.e.m. of three independently collected MST traces. See Figs EV5 and EV6 for MST raw data.

Source data are available online for this figure.

within 30 min of CHX treatment in *alf4*, whereas the protein was degraded to 60% of its initial levels in the wild type (Fig 4A and B).

To determine the role of ALF4 in Aux/IAA degradation, we used a *pDEX:IAA17-GFP* construct to examine IAA17 levels after auxin treatment in *alf4-1* compared to wild-type controls. After a 4-h dexamethasone treatment, the amount of IAA17-GFP was clearly higher in the root tip of *alf4-1* plants compared to the wild type (Fig 4C and D). Examination of IAA17-GFP levels after auxin treatment revealed that the protein was relatively stable in *alf4-1* plants compared to the wild type. Importantly, *IAA7-GFP* transcript abundance was similar in the two lines. Because accumulation of Aux/IAA proteins results in auxin resistance, these results are consistent with reduced auxin response observed in the *alf4* mutant (Salehin *et al*, 2015).

If ALF4 functions like GLMN and inhibits CRL activity, it is counterintuitive that SCF substrates should be stabilized in the *alf4* mutant. One possibility is that loss of ALF4 leads to changes in the abundance of SCF subunits. To assess this possibility, we first examined CUL1 levels in wild-type and *alf4-1* plants, in the absence and presence of the proteasome inhibitor MG132. The immunoblot in Fig 5A shows that the levels of unmodified and neddylated CUL1 are reduced in the mutant compared to the wild type. Treatment with MG132 increased the amount of both forms in the mutant and wild type, indicating that CUL1 is a substrate for the proteasome. However, we note that CUL1 levels in *alf4* plants are not restored to wild-type levels by MG132. To determine whether CUL1 stability is affected in the mutant, we treated
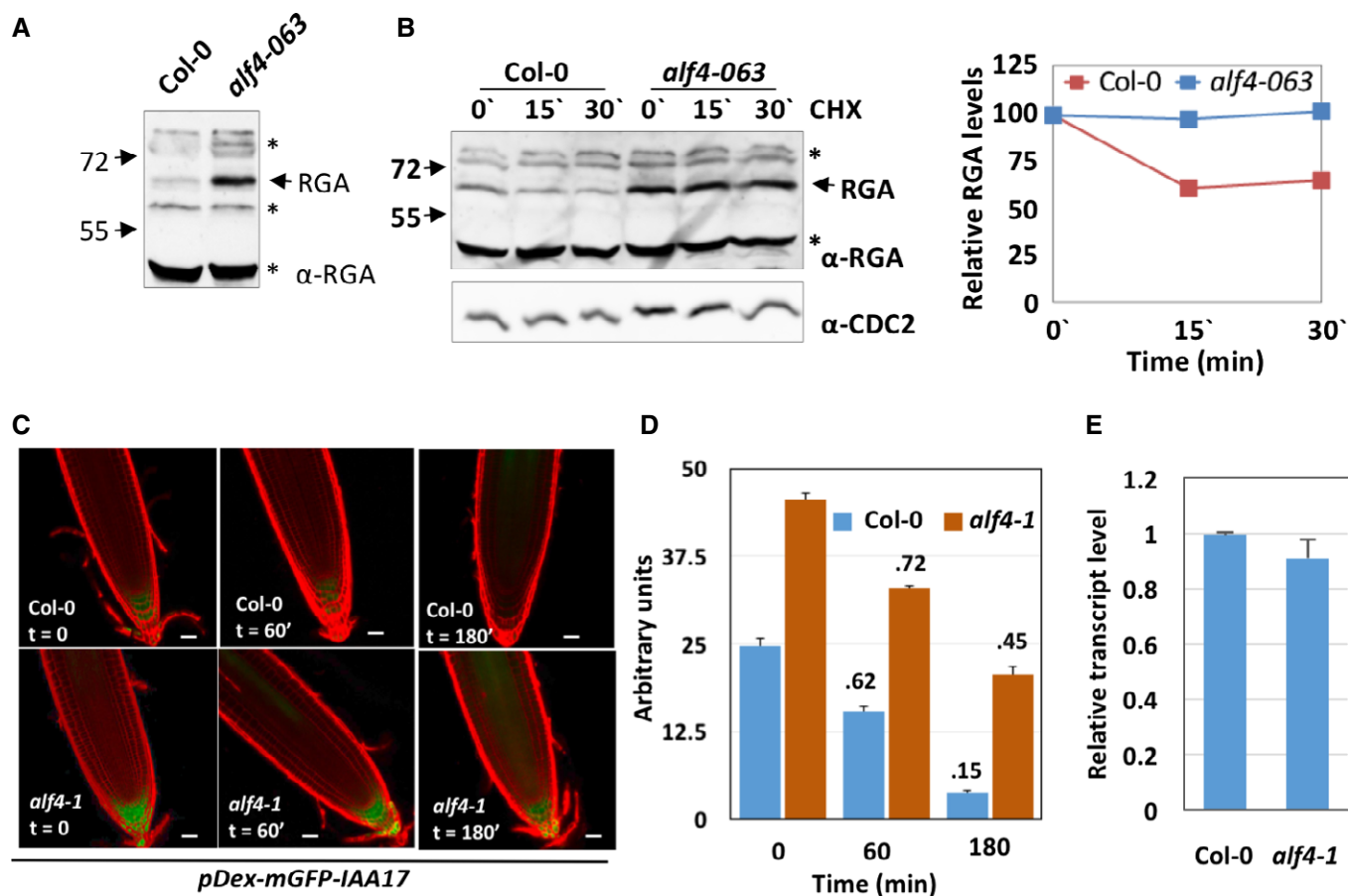

Figure 4. SCF substrates accumulate in the *alf4* mutant.

A   Total protein extracts prepared from 13-day-old wild-type and *alf4-063* seedlings, separated by SDS–PAGE, and probed with anti-RGA antibody. Background cross-reacting bands are indicated by asterisks.

B   8-day-old wild-type and mutant seedlings were treated with 50 μM cycloheximide (CHX) for up to 30 min as indicated in the figure. Total protein extracts were separated by SDS–PAGE and probed with anti-RGA antibody. Asterisks indicate background cross-reacting bands. The anti-CDC2 immunoblot serves as loading control. Relative RGA signal intensity was measured using MultiGAUGE and plotted on the right.

C   Confocal images showing IAA17-GFP levels in wild-type and *alf4-1* roots. Seedlings were treated with 5 μM dexamethasone for 4 h followed by treatment with 10 μM IAA for the indicated time. Scale bars are 50 μm.

D   IAA17-GFP levels measured using ImageJ software. Data were collected from 4 roots for each time point. Error bars represent standard deviation. The difference between Col-0 and *alf4-1* is significant $P < 0.001$, Student's *t*-test (two-tailed) for each of the time points (t = 0, t = 60′ and t = 180′). Values above the bar are the fraction of IAA17-GFP remaining relative to time zero.

E   Relative *IAA17-GFP* transcript levels in 7-day-old seedlings after treatment with dexamethasone for 4 h. Data shown are from three biological replicates. Error bars represent standard deviation. Differences are not significant, Student's *t*-test (two-tailed).

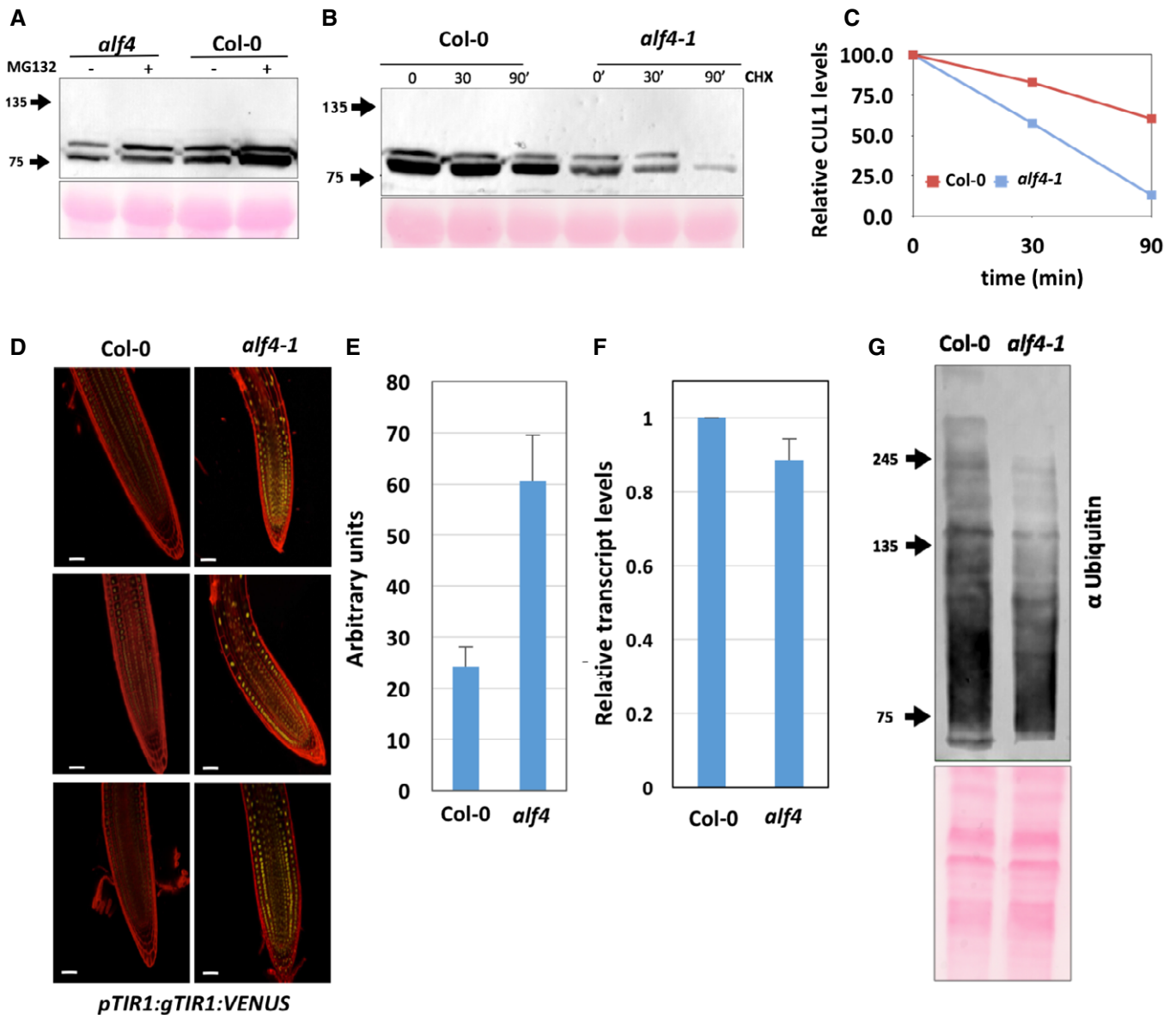Source data are available online for this figure.

Figure 5. Stability of SCF subunits of the *alf4* mutant.

A Total protein extracts prepared from 7-day-old wild-type and *alf4-1* seedlings treated or untreated with 100 μM MG132 were separated by SDS–PAGE and probed with anti-CUL1 antibody. The bands are CUL1 and CUL1 modified with NEDD8.

B 7-day-old wild-type and *alf4*-1 mutant seedlings were treated with 200 μM cycloheximide (CHX) for up to 90 min as indicated. Total protein extracts were separated by SDS–PAGE and probed with anti-CUL1 antibody. Total protein stained with Ponceau S served as loading control.

C Immunoblot was used to quantify CUL1 protein levels in wild-type and mutant plants using ImageJ. The levels of unmodified CUL1 are expressed relative to Ponceau S-stained Rubisco large subunit.

D Confocal images showing root tip regions of representative 7-day-old *pTIR1:gTIR1-VENUS* and *alf4-1 pTIR1:gTIR1-VENUS* seedlings. Scale bars are 50 μm.

E TIR1-VENUS protein levels in wild-type and mutant plants measured with ImageJ. Error bars represent standard deviation ($n = 7$ plants). Difference between Col-0 and *alf4-1* is significant $P < 0.001$, Student's t-test (two-tailed).

F Relative transcript level of *TIR1-Venus* was measured in wild-type and *alf4-1* lines by qRT–PCR. Data are from three biological replicates. Error bars represent standard deviation. Differences are not significant, Student's t-test (two-tailed).

G Immunoblot of total protein from 7-day-old wild type and *alf4-1* probed with anti-ubiquitin antibody. The experiment was repeated twice with similar results.

Source data are available online for this figure.

seedlings with CHX and collected samples at time intervals thereafter. The data in Fig 5B and C show that CUL1 stability is substantially reduced in the mutant. In contrast, we find that TIR1 abundance, as detected by examining a fusion of TIR1 to the fluorescent protein VENUS, are increased in the mutant (Fig 5D and E). Since *TIR1-VENUS* transcript accumulation is not affected in the mutant (Fig 5F), the increase in protein levels is probably due to increased stability.

Since RBX1 functions in all CRL E3 ligases, it is possible that the *alf4* mutants have a broad defect in ubiquitin–protein conjugation. To assess this possibility, we performed an immunoblot of total cellular proteins with an anti-ubiquitin antibody. Indeed, the results in Fig 5G show a general decrease in the amount of ubiquitinated proteins in the *alf4-1* mutant.

SCF^{TIR1}-dependent degradation of Aux/IAA proteins is inhibited by ALF4

Based on the known function of the GLMN protein, we hypothesized that the ALF4–RBX1 interaction may influence the access of ubiquitin-charged E2s (E2~Ub) to RBX1, and therefore the ubiquitination of SCF targets. To determine whether this was the case, we established an *in vitro* assay utilizing human ubiquitin-activating enzyme (UBE1), the *Arabidopsis* conjugating enzyme AtUBC8, ubiquitin, and the RING domain of RBX1 (RBX1^{RING}). Previous studies have shown that the RING domain is sufficient to promote protein ubiquitination in these conditions (Hardtke *et al*, 2002; Voiniciuc *et al*, 2013). The data in Fig 6A demonstrate this activity and show that the reaction is E2- and RBX1^{RING}-dependent. The introduction of wild-type ALF4 strongly inhibited the ubiquitination reaction (Fig 6A). Further, and consistent with our earlier results, neither ALF4^{A484A614} nor ALF4$^{1-532stop}$ had a significant effect on the reaction.

To further explore the impact of ALF4 on SCF activity, we reconstituted E1-E2-SCF^{TIR1}-mediated ubiquitination of Aux/IAAs in an *in vitro* ubiquitination system (IVU) as previously described (Winkler *et al*, 2017). All the components of the enzyme cascade are included in this assay including E1 (UBA1), the E2 AtUBC8, the E3 SCF^{TIR1}, and the substrate GST-IAA7 (Fig EV7A). As expected, we found that GST-IAA7 ubiquitination is mediated by SCF^{TIR1} in an auxin- and time-dependent manner (Fig 6B and D). The addition of excess ALF4 to the IVU reactions prevented the formation of IAA7–ubiquitin conjugates (Fig 6B). Further, the addition of increasing amounts of ALF4 resulted in a concentration-dependent decrease in the levels of ubiquitinated IAA7 (Fig 6C).

In human cells, GLMN inhibits the activity of SCF^{FBW7} by masking the E2 binding face of RBX1 (Duda *et al*, 2012). To determine whether ALF4 acted in a similar way, we examined the effects of increased E2 protein on SCF^{TIR1} activity (Fig 6D). In the absence of ALF4, the addition of higher levels of E2 stimulated the formation of IAA7–ubiquitin. This effect was also observed in the presence of ALF4, indicating that E2 and ALF4 exert counteracting effects on IAA7 ubiquitination. Taken together with our other results, these findings indicate that ALF4 probably inhibits SCF activity by competing with the E2 for binding to RBX1.

Discussion

The ubiquitin-proteasome system is a complex and highly regulated network that mediates the degradation of thousands of proteins (Vierstra, 2009). In general, degradation of specific substrates is regulated at the level of substrate recognition. However, the activities of E3 ligases are also directly regulated in a number of ways (Vittal *et al*, 2015). In the case of the CRLs, the E3 is activated by neddylation of the cullin subunit and inhibited by the CSN and CAND1 proteins. Typical for the ubiquitin system, these

components are highly conserved and their loss can result in lethality in plants and animals. Here, we show that the *Arabidopsis* ALF4 protein, similar to human GLMN, inhibits SCF E3 ligases. Like GLMN, ALF4 binds to the RBX1 subunit of the SCF likely preventing the interaction between the E2 and RBX1.

Although the similarity between ALF4 and GLMN is low at the sequence level, several key residues required for interaction with RBX1 are conserved. In addition, modeling of the ALF4 structure indicates that ALF4 consists of a series of helical repeats similar to the HEAT repeats of GLMN. By analogy with the published GLMN structure, the C-terminus of ALF4 probably interacts with RBX1. Indeed, a truncated ALF4 lacking 94 amino acids at the C-terminus of the protein is deficient in RBX1 binding. Further, substitution of the conserved residues K484 and K614 with alanine greatly reduces both RBX1 binding and activity *in vitro*. MST also demonstrates that ALF4 binds to RBX1. Although the affinity constant for ALF4–MmRBX1–HsCUL1 binding is about ten times higher than that previously found for the GLMN–MmRBX1–HsCul1 interaction, this difference is likely due to the cross-species nature of the proteins we used for MST (Duda *et al*, 2012). Finally, the proposed activity of ALF4 is supported by our demonstration that ALF4 inhibits general RBX1-dependent ubiquitination as well as TIR1-dependent ubiquitination of the SCF^{TIR1} substrate IAA7.

We find that the SCF substrates RGA and IAA17 are stabilized in the *alf4* mutant compared to the wild-type control. This is counterintuitive since loss of an SCF inhibitor should result in decreased substrate levels. However, this result is consistent with previous studies of CRL regulators. For example, in *Arabidopsis*, a decrease in abundance of the CSN results in accumulation of NEDD8-modified CUL1 relative to the wild type, consistent with the de-neddylating activity of the CSN. This change is associated with a decrease in the amount of TIR1, probably because of increased autocatalytic degradation of the F-box protein, and a corresponding increase in SCF substrates (Schwechheimer *et al*, 2001; del Pozo *et al*, 2002; Stuttmann *et al*, 2009a,b). In the case of the *alf4* mutants, we also find that the levels of CUL1 are decreased. However, in this case, and unlike the *csn* mutants, both modified and unmodified CUL1 abundance is reduced. Paradoxically, we find that the level of TIR1 is increased in the *alf4* mutant. We speculate that this may be because neddylated CUL1 is limiting in the mutant so that a larger fraction of the TIR1 pool is not assembled into an SCF and therefore not subject to autocatalytic degradation. This idea is supported by our earlier studies showing that TIR1 is unstable when assembled into an SCF complex (Yu *et al*, 2015). One important question is why CUL1 is less stable in *alf4* plants. This may be because the loss of ALF4 results in an increase in autocatalytic ubiquitination and degradation. However, our results with MG132 are not consistent with this idea. CUL1 is clearly degraded by the proteasome but if decreased CUL1 stability in *alf4* is proteasome dependent, we would expect MG132 treatment would restore CUL1 amounts to near wild-type levels. The fact that it does not leaves open the possibility that another protease is involved. Further experiments will be required to resolve this issue.

Accumulation of IAA17 and RGA, as well as other members of the DELLA and Aux/IAA families, may be responsible for many aspects of the *alf4* growth phenotype. However, since CUL1 is found in all SCF complexes, it is likely that most, perhaps all, SCFs are affected by the loss of ALF4. This is consistent with our observation
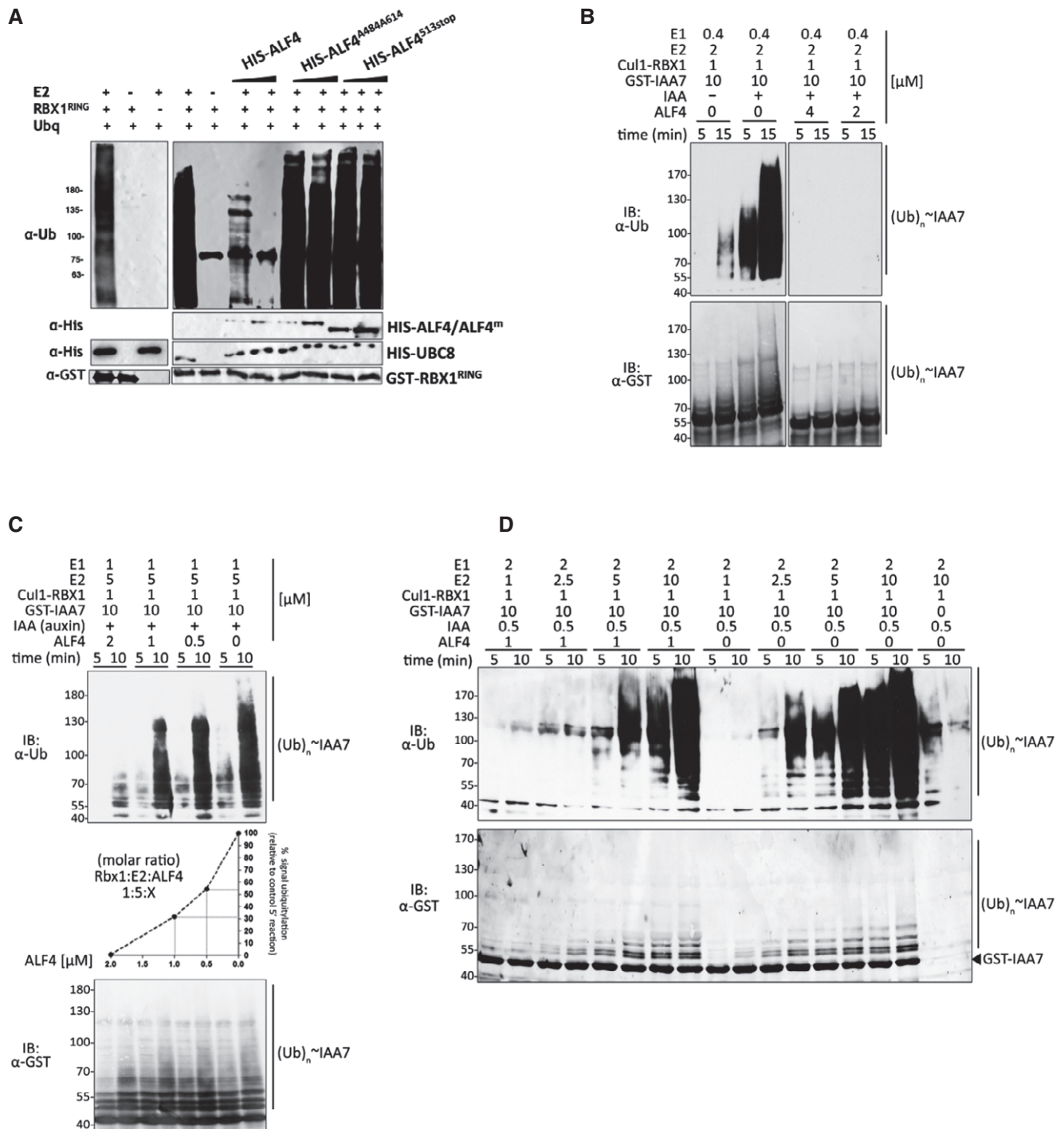
Figure 6. ALF4 inhibits SCF^TIR1 E3 ligase activity.

A   Ubiquitination assays including 6xHis-At-UBA1 (E1), 6xHis-At-UBC8 (E2), GST-RBX1^RING, and ubiquitin (Ub) in the presence and absence of 6xHIS-ALF4 protein were performed. The reactions were separated by SDS–PAGE and probed with anti-ubiquitin antibody.

B–D   SCF^TIR1- and auxin-dependent transfer of ubiquitin to GST-IAA7 protein. Each reaction consists of UBA1 (E1), UBC8 (E2), ubiquitin, Cul1–RBX1, TIR1-ASK1, GST-IAA7, and various amounts of ALF4. Immunoblots with either anti-ubiquitin or anti-GST antibodies show IAA7–ubiquitin conjugates. Numbers to the left of the blots indicate protein size (in kDa). (B) Rapid (5 and 15 min) inhibition of GST-IAA7 ubiquitination occurs in the presence of ALF4. (C) ALF4 inhibits GST-IAA7 ubiquitination in a concentration-dependent manner. The levels of ubiquitin–protein conjugates are expressed relative to the 5-min reaction without ALF4 control. (D) Increasing levels of E2 reduce the effects of ALF4 on ubiquitination of IAA7. Ubiquitin conjugates on target proteins were detected as above, while anti-GST and anti-mouse-Alexa 647 antibodies were used for the detection of specific ubiquitin species on GST-IAA7. The last two lanes in the immunoblots correspond to reactions (5–10 min) containing all IVU components and GST (instead of GST-IAA7) as a control.

Source data are available online for this figure.

that the *alf4* mutation causes a general decrease in the level of ubiquitinated proteins. Whether ALF4 regulates CUL3- and CUL4-based CRLs remains to be explored. Surprisingly, the *glmn* mutation in human cells appears to have a somewhat specific effect on SCF[Fbw7] (Tron *et al*, 2012). The basis for this specificity is currently unknown. One possibility is that GLMN regulates the activity of a specific pool of CRLs, perhaps defined by its subcellular distribution.

Previous reports demonstrated that the *alf4* mutants are deficient in the early divisions of pericycle cells during lateral root formation. Although auxin is required at this stage of the process, it was proposed that ALF4 functions independently of auxin (DiDonato *et al*, 2004). Here, we show that *alf4* is resistant to auxin and displays reduced *pDR5:GFP* activity, suggesting that reduced auxin response contributes to the lateral root defect. We also observe a strong rosette and inflorescence phenotype in *alf4-1*. The *alf4-2* and *alf4-063* mutants are extremely small and slow-growing and rarely survive to flower. Grafting experiments suggest that a reduced root system contributes to the aerial phenotype, but nevertheless, the ALF4 protein is clearly required in the rosette and inflorescence. Thus, like GLMN in mouse, ALF4 appears to be essential for viability.

Although CRLs are activated or inhibited by several factors including NEDD8, the CSN, and now ALF4/GLMN, how these factors are regulated remains an open question. The CSN is released from the SCF by the presence of substrate, at least *in vitro* (Enchev *et al*, 2012). Presumably ALF4 is released from the SCF under appropriate conditions, perhaps in response to increased E2 levels or by an increase in substrate levels. A recent report also demonstrated that *ALF4* transcription is regulated by very long-chain fatty acids (Shang *et al*, 2016). These molecules are thought to restrict the ability of pericycle cells to form callus tissue, possibly by repressing transcription of *ALF4*. In the future, it will be interesting to determine whether *ALF4* is regulated by other signaling pathways.

Materials and Methods

Plant material, growth conditions, and microscopy

Previously published *alf4-1* (Celenza *et al*, 1995), *alf4-063* (SALK_063183) (DiDonato *et al*, 2004), *pALF4:ALF4-GFP* (DiDonato *et al*, 2004), and *pDR5rev:GFP-ER* (Friml *et al*, 2003) are in the Col-0 background. *pARR5:GFP* (Yanai *et al*, 2005) is in the Ws background. *alf4-2* (SALK_089074) is a newly described allele in the Col-0 background and was obtained from the Nottingham *Arabidopsis* Seed Centre. *Alf4* allele mutation sites were mapped using the primers in Table EV1. Further information on *alf4* alleles is shown in Fig EV1. For grafting, root growth assays, and confocal imaging, plants were grown vertically on MS plates with 1% bacto agar (no sucrose) under short day conditions (8 h of 80–100 μmol/m²/s light) at 20°C. Seven days after germination, plants were grafted according to a previously published protocol (Melnyk *et al*, 2015). Ten days after grafting, grafted plants and non-grafted controls were moved into soil under long day conditions (16 h of 120 μmol/m²/s light) at 20°C. Care was taken to select successful grafts, indicated by the presence of lateral root growth and the absence of adventitious root formation at 10 days. For hormone treatment of *pDR5:GFP* and *pARR5:GFP*

lines, 8-day-old plants were transferred onto MS media containing DMSO, 0.08 μM BA, or 1 μM NAA. After 24 h, plants were stained with propidium iodide and imaged on a Zeiss LSM-700 laser confocal scanning microscope. For ALF4-GFP imaging, 10-day-old plants were stained with propidium iodide and imaged on a LSM-700 microscope. For *pALF4:ALF4-GFP* hormone treatments, 5-day-old plants were transferred onto 1/2MS media containing DMSO, 0.08 μM BA, 1 μM NAA, or 5 μM NPA and after 48 h imaged on an LSM-700 microscope. Image quantifications for *pDR5:GFP* and *pARR5:GFP* lines were done on the entire image using the mean function on FIJI (fiji.sc). Brightness was adjusted for controls and samples equally. For immunoblot analysis of RGA, seedlings were grown on full MS media for 8 or 13 days. CHX treatment was performed in liquid GM supplemented with 50 μM CHX. To generate *pDex:IAA17-GFP* plants, *IAA17* CDs was PCR-amplified and cloned into Sfi1A and Sfi1B sites of pENTR-D-GFP vector and subsequently cloned into binary vector *pDexSalkOne* using LR Gateway reaction (Invitrogen 11791). The resulting *pDex-mGFP-IAA17* clone was transformed into Agrobacterium GV3101 strain and transformed into Col-0 plants by floral dip (Clough & Bent, 1998). Independent T3 lines were obtained by hygromycin selection.

Plasmid construction

Two *ALF4* isoforms were used in this study. The majority of the data were generated using UniProt isoform 1 (Q84VX3-1) which is 626 amino acids. The data in Figs 6B and C, and EV7A were generated using a shorter isoform (F4JWD6), which lacks exon 9 and an N-terminal extension. The two isoforms generated similar results in biochemical studies. cDNAs were cloned into *pENTRdTOPO* vector (Invitrogen K2400). Full-length *ALF4* cDNA was amplified by polymerase chain reaction using primers *ALF4_FL/GW-F* and *ALF4_FL-R*. *ALF4*[A484,A614] cDNA was amplified using *ALF4 K484A_F* and *ALF4 K484A_R* followed by *ALF4R614A_F* and *ALF4R614A_R*. *ALF4*[1-532stop] was generated with primers *ALF4_FL/GW-F* and *ALF4FL*[532stop]*-R*. Similarly, RBX1 cDNA was amplified using primers RBX1_F/GW and RBX1_REV. The RBX1 ring domain (RBX1[RING]) was amplified using primer set RBX1-142F and RBX1_REV. These entry clones were then further subcloned into different destination vectors using Gateway® LR technology (Invitrogen 11791).

Auxin root growth assay

The effects of exogenous auxin IAA on root growth were determined as described in Prigge *et al* (2016). Surface-sterilized wild-type and *alf4-1* seeds were placed on vertically oriented 1/2 strength MS plates with 1% bacto agar under long day conditions (16-h light and 8-h dark) in a growth chamber (80 μmol/m²/s, 22°C). Five-day-old seedlings of similar size were then transferred to new plates supplemented with various concentrations of auxin. After 3 days, the amount of new root growth was measured and the percentage root growth inhibition was calculated relative to root growth on minimal medium minus hormone.

Gravitropic assay

To determine the response of roots to gravity, wild-type and *alf4-1* seedlings were germinated and grown for 3 days on MS medium

under long day conditions. Plants of similar size were selected and transferred to square petri dish containing the same media and grown for a day before being rotated by 90°. To measure root re-orientation, the plates were scanned at regular time intervals. Root angle was measured using ImageJ.

Yeast two-hybrid assay

For yeast two-hybrid assays, full-length *ALF4* cDNA as well as mutant versions were ligated into the *pGILDA* vector (Clontech), while the *RBX1* cDNA was inserted into the *pB42AD* plasmid (Clontech) and transformed into *Escherichia coli* competent cells. Bait and prey constructs were co-transformed into *Saccharomyces cerevisae* strain EGY48 (Clontech), and transformants were selected on SD supplemented with –Ura/–His/–Trp drop-out solution (BD Biosciences) and glucose medium. To test the interaction between ALF4 or ALF4 mutants with RBX1, yeast colonies that grew fastest were plated on SD-galactose/raffinose inducing medium containing –Ura/–His/–Trp drop-out supplement containing 80 µg/ml X-Gal (5-bromo-4-chloro-indolyl-b-D-galactopyranoside).

Bimolecular fluorescence complementation (BiFC)

For the BiFC assay, *ALF4* or *ALF4* mutant cDNAs were cloned into destination vectors pDEST–VYCE(R) (Gehl *et al*, 2009), while *RBX1* cDNA was cloned into pDEST–VYNE(R) (Gehl *et al*, 2009). These binary vectors were transferred into *Agrobacterium tumefaciens* strain GV3101 (pMP90). For transient expression, *A. tumefaciens* strains carrying the BiFC constructs were used together with the p19 strain for infiltration of 5- to 6-week-old *Nicotiana benthamiana* leaves. Fluorescence of the lower epidermis of leaf disks 2–5 days after infiltration was visualized with the confocal laser scanning microscope.

Confocal microscopy

Confocal imaging of plant roots shown in Figs 4C and 5D was performed using a Zeiss LSM 710 microscope. To visualize primary root tips, they were counterstained in 10 mg/l propidium iodide for 1–2 min, rinsed, and mounted in water. ImageJ was used to quantify the intensity of YFP or GFP fluorescence signal.

qRT–PCR

RNA was extracted from 7-day-old seedlings using the RNeasy plant mini kit (Qiagen), and the yield was quantified using a NanoDrop spectrophotometer. A total of 500 ng of total RNA was used for DNase I treatment (Ambion) and then reverse-transcribed using a poly-dT primer and the Superscript III First Strand cDNA Synthesis System for RT–PCR (Invitrogen). Quantitative PCR was performed on a CFX96 Real-Time System (Bio-Rad). RNA levels were normalized against transcripts of the GAPC2 gene (AT1G13440). The oligos used for PCR are listed in Table EV1.

Protein expression, purification, and analysis

Using the Gateway® cloning technology, coding sequences of *At*ALF4 (Q84VX3-1 and F4JWD6) were cloned into the pDEST™17

vector (ThermoFisher Scientific) as an N-terminal 6× histidine fusion. The ALF4 fusion protein was expressed in *E. coli* BL21 (DE3) cells grown in 2× YT medium. *Escherichia coli* cells with an OD600 = 0.8–1 were induced with 0.6 mM IPTG after a 20-min cold shock. After 6-h incubation at 25°C, cells were harvested by centrifugation (6,000 × *g*, 20 min, 4°C). For lysis, 5 ml lysis buffer (50 mM Tris–HCl pH 8.0, 200 mM NaCl, 10 mM imidazole, complete EDTA-free protease inhibitor cocktail (Roche), 2 mM DTT, 1 PMSF) per gram pellet was added and the cell suspension was sonicated (3 × 2 min, 1 s pulse/1 s pause). The lysate was clarified by centrifugation at 50,000 × *g* for 20 min at 4°C and applied to an Äkta pure FPLC system (GE Healthcare) for purification. As a first affinity purification step, the lysate was loaded to a pre-equilibrated (50 mM Tris–HCl pH 8.0, 200 mM NaCl, 10 mM imidazole, 2 mM DTT) 1 ml Protino® Ni-NTA (Macherey-Nagel) column, and eluted via a 10–400 mM imidazole gradient. ALF4 protein peaks were combined, and for an anion exchange (anIEX) purification step, a buffer exchange was carried out to 50 mM Tris–HCl pH 8.0, 50 mM NaCl, 2 mM DTT, with a 30-kDa cut-off centricon (Amicon). AnIEX purification was performed with a MonoQ 5/50 GL (GE Healthcare) column, and the protein was eluted by a gradient from 50 to 500 mM NaCl. All ALF4-containing fractions were combined, concentrated to a volume of 2–3 ml, and applied directly into a HiLoad S200 16/60 PG size exclusion chromatography (SEC) column. ALF4 protein was eluted with 50 mM Tris–HCl pH 8.0, 200 mM NaCl, 2 mM DTT at a flow rate of 1 ml/min. Upon SEC, two species of ALF4 eluted: one at a retention volume of ~45 ml and second one around 65 ml. All ALF4-containing fractions were combined, concentrated, and stored in storage buffer (50 mM Tris–HCl pH 8.0, 200 mM NaCl, 2 mM DTT, 10% (v/v) glycerol) at −80°C after being flash-frozen in liquid nitrogen. Preparation of recombinant expressed GST-tagged ASK1–TIR1 protein complex from SF9 insect cells, GST-tagged HsCul1–MmRBX1 (split'n coexpress system), 6xHis-UBA1, and 6xHis-UBC8 from *E. coli* was performed as previously published (Tan *et al*, 2007; Calderon Villalobos *et al*, 2012; Winkler *et al*, 2017).

Plant protein extraction and analysis

Seedlings of the indicated age were harvested and ground to a fine powder in liquid nitrogen followed by extraction in plant buffer containing 50 mM Tris pH 7.5, 150 mM NaCl, 10% glycerol, 0.1% NP-40, complete protease inhibitor (Roche), and 20 µM MG-132. Cellular debris was removed by centrifugation and total protein concentration was quantified by BCA (Thermo scientific) or Bradford assay. Samples were separated by SDS–PAGE followed by transfer to nitrocellulose membrane (Amersham). Blots were then incubated with anti-ASK antibody (1:1,000), anti-ubiquitin antibody (1:1,000; VWR International), anti-RGA antibody (1:1,000; Willige *et al*, 2007), and anti-CDC2 antibody (1:5,000; Santa Cruz Biotechnology), to detect the recovered proteins. Membranes were visualized using ECL Plus or Super Signal Western Blot Detection System (GE healthcare).

For the immunoprecipitation assays, total proteins were extracted from 2-week-old seedlings expressing *pALF4:ALF4-GFP* and *pEF1a:GFP* (Meckfessel *et al*, 2012). 15 µl of anti-GFP polyclonal antibody (Invitrogen) was crosslinked by BS3 (Thermo Scientific Pierce, P121580) to Protein G Dynabeads (Life Technologies,

10004D) and incubated with 10 mg of total proteins for 4 h at 4°C. The complexes were washed several times and then applied to SDS–PAGE for immunoblot detection. Rabbit anti-RBX1/ROC1 polyclonal antibody (Thermo Fisher AHO0402), raised against the synthetic peptide CysPLDNREWEFQKYGH, was used at 1:1,000 dilution to detect RBX1 protein.

RBX1-based *in vitro* ubiquitination assay

RBX1-dependent ubiquitination assays were performed in 30 μl reactions containing 50 mM Tris–HCl, pH 7.5, 10 mM MgCl$_2$, 1 mM ATP, 0.05 mM ZnCl$_2$, 0.2 mM DTT, 10 mM phosphocreatine, phosphocreatine kinase (0.1 units), 100 ng 6xHis-UBE1 (E1) (BostonBiochem), 250 ng 6xHis-UBC8 (E2), 2 μg ubiquitin (BostonBiochem), 250 ng GST-RBX1^{RING}, in the presence or absence of 100 ng of ALF4. Similar reactions without the E2 enzyme or RBX1 were used as controls. RBX1 was synthesized as previously described (Voiniciuc *et al*, 2013). The reactions were incubated at 30°C for 2 h or at different time interval. The reaction was stopped by the addition of reducing loading buffer. Samples were then loaded and separated by SDS–PAGE, blotted onto nitrocellulose membrane, and analyzed using anti-ubiquitin antibody (VWR International) at a dilution of 1:1,000. Membranes were visualized using the ECL Plus Western Blot Detection System (GE healthcare).

SCF^{TIR1}-dependent ubiquitination assay

In vitro ubiquitination assays (IVUs) were carried out as recently described (Winkler *et al*, 2017). In brief, UBA1 (E1) and UBC8 (E2) were incubated with different concentrations of highly purified ALF4, and mixed with pre-assembled SCF^{TIR1} (E3) and GST-IAA7 with or without IAA (auxin). IVU samples were incubated at 25°C, 500 rpm, aliquots were taken at specified time points, and ubiquitin chain formation was stopped by the addition of 4× Laemmli buffer and denaturation 5 min 95°C. Either 8% or 5–15% acrylamide gradient gels were used for separation of ubiquitinated samples. For the detection of ubiquitinated species, immunoblotting was performed using primary anti-ubiquitin in mouse (1:500 or 1:2,000, P4D1, Santa Cruz), and anti-GST in rabbit (1:20,000, G7781, SIGMA) antibodies, followed by anti-mouse HRP (1:10,000, Thermo Fischer Scientific), and anti-rabbit AP (1:10,000, Sigma-Aldrich) or anti-rabbit Alexa Fluor Plus 647 (1:35,000, A32733, Thermo Fischer Scientific) secondary antibodies. Nitrocellulose membranes were scanned using a Typhoon FLA9500 system (473-nm excitation wavelength and LPB filter) or incubated with either alkaline phosphatase or ECL substrates.

Microscale thermophoresis

5 μM HsCul1–MmRbx1 was labeled using the Monolith NTTM Protein Labeling Kit RED-NHS (Nanotemper Technologies) according to the manufacturer's protocol. The dye/protein ratio used was 10:1. Free dye was removed with the supplied buffer exchange column using MST analysis buffer (50 mM Tris–HCl pH 7.5, 150 mM NaCl, 10 mM MgCl$_2$, 0.05% (v/v) Tween-20). Labeling efficiency was determined by measuring absorbance at 280 and 650 nm and using Beer–Lambert law for concentration determination. Labeled Cul1–RBX1 protein sample was adjusted to

20 nM with the MST analysis buffer (see above). ALF4 was centrifuged for 10 min (21,000 × *g*, 4°C) and used in a 16 step 1:1 dilution series in MST analysis buffer containing 1 mg/ml BSA. ALF4 concentrations from 14 μM to 0.42 nM were set up and included in the MST experiment. For thermophoresis measurements, Cul1–RBX1-labeled protein sample was mixed 1:1 with each of the ALF4 dilution series which results in 10 nM labeled Cul1–RBX1, and 7 μM–0.21 nM ALF4 concentrations. After 5-min incubation at room temperature, each dilution was filled into Monolith NTTM MST Premium-coated capillaries (Nanotemper Technologies). A capillary scan was performed with 20% LED power, while MST measurements for affinity were performed at 20 and 40% LED power in a Monolith NT.115 (Nanotemper Technologies). For analysis, the data of three independently generated measurements with different protein preparations (biological replicates) at 40% LED power were used, applying the signal from Thermophoresis + T-Jump in the NT Affinity Analysis software version 2.0.2.

Expanded View for this article is available online.

Author contributions

RB and CWM characterized the mutant. CWM examined *ALF4* gene expression. RB performed Y2H, *in vitro* pulldown and BiFC experiments. GC and MW performed MST experiments. GC, MW, and MN carried out SCF^{TIR1}-based ubiquitination assays. RB and JM examined the levels of SCF subunits and substrates. KK and MS provided reagents. RB, CWM, GC, MW, CS, LIACV, and ME designed the experiments. RB, CWM, CS, LIACV, and ME wrote the paper.

Conflict of interest

The authors declare that they have no conflict of interest.

References

Calderon Villalobos LI, Lee S, De Oliveira C, Ivetac A, Brandt W, Armitage L, Sheard LB, Tan X, Parry G, Mao H, Zheng N, Napier R, Kepinski S, Estelle M (2012) A combinatorial TIR1/AFB-Aux/IAA co-receptor system for differential sensing of auxin. *Nat Chem Biol* 8: 477–485

Celenza JL Jr, Grisafi PL, Fink GR (1995) A pathway for lateral root formation in *Arabidopsis thaliana*. *Genes Dev* 9: 2131–2142

Chupeau MC, Granier F, Pichon O, Renou JP, Gaudin V, Chupeau Y (2013) Characterization of the early events leading to totipotency in an *Arabidopsis* protoplast liquid culture by temporal transcript profiling. *Plant Cell* 25: 2444–2463

Clough SJ, Bent AF (1998) Floral dip: a simplified method for *Agrobacterium*-mediated transformation of *Arabidopsis thaliana*. *Plant J* 16: 735–743

Deshaies RJ, Joazeiro CA (2009) RING domain E3 ubiquitin ligases. *Annu Rev Biochem* 78: 399−434

DiDonato RJ, Arbuckle E, Buker S, Sheets J, Tobar J, Totong R, Grisafi P, Fink GR, Celenza JL (2004) *Arabidopsis* ALF4 encodes a nuclear-localized protein required for lateral root formation. *Plant J* 37: 340−353

Duda DM, Borg LA, Scott DC, Hunt HW, Hammel M, Schulman BA (2008) Structural insights into NEDD8 activation of cullin-RING ligases: conformational control of conjugation. *Cell* 134: 995−1006

Duda DM, Olszewski JL, Tron AE, Hammel M, Lambert LJ, Waddell MB, Mittag T, DeCaprio JA, Schulman BA (2012) Structure of a glomulin-RBX1-CUL1 complex: inhibition of a RING E3 ligase through masking of its E2-binding surface. *Mol Cell* 47: 371−382

Enchev RI, Scott DC, da Fonseca PC, Schreiber A, Monda JK, Schulman BA, Peter M, Morris EP (2012) Structural basis for a reciprocal regulation between SCF and CSN. *Cell Rep* 2: 616−627

Friml J, Vieten A, Sauer M, Weijers D, Schwarz H, Hamann T, Offringa R, Jurgens G (2003) Efflux-dependent auxin gradients establish the apical-basal axis of *Arabidopsis*. *Nature* 426: 147−153

Gagne JM, Downes BP, Shiu SH, Durski AM, Vierstra RD (2002) The F-box subunit of the SCF E3 complex is encoded by a diverse superfamily of genes in *Arabidopsis*. *Proc Natl Acad Sci USA* 99: 11519−11524

Gehl C, Waadt R, Kudla J, Mendel RR, Hansch R (2009) New GATEWAY vectors for high throughput analyses of protein-protein interactions by bimolecular fluorescence complementation. *Mol Plant* 2: 1051−1058

Gilkerson J, Hu J, Brown J, Jones A, Sun TP, Callis J (2009) Isolation and characterization of cul1-7, a recessive allele of CULLIN1 that disrupts SCF function at the C terminus of CUL1 in *Arabidopsis thaliana*. *Genetics* 181: 945−963

Hardtke CS, Okamoto H, Stoop-Myer C, Deng XW (2002) Biochemical evidence for ubiquitin ligase activity of the *Arabidopsis* COP1 interacting protein 8 (CIP8). *Plant J* 30: 385−394

Hua Z, Vierstra RD (2011) The cullin-RING ubiquitin-protein ligases. *Annu Rev Plant Biol* 62: 299−334

Kelley DR, Estelle M (2012) Ubiquitin-mediated control of plant hormone signaling. *Plant Physiol* 160: 47−55

Kelley LA, Mezulis S, Yates CM, Wass MN, Sternberg MJ (2015) The Phyre2 web portal for protein modeling, prediction and analysis. *Nat Protoc* 10: 845−858

Lavy M, Estelle M (2016) Mechanisms of auxin signaling. *Development* 143: 3226−3229

Li T, Pavletich NP, Schulman BA, Zheng N (2005) High-level expression and purification of recombinant SCF ubiquitin ligases. *Methods Enzymol* 398: 125−142

Lydeard JR, Schulman BA, Harper JW (2013) Building and remodelling Cullin-RING E3 ubiquitin ligases. *EMBO Rep* 14: 1050−1061

Meckfessel MH, Blancaflor EB, Plunkett M, Dong Q, Dickstein R (2012) Multiple domains in MtENOD8 protein including the signal peptide target it to the symbiosome. *Plant Physiol* 159: 299−310

Melnyk CW, Schuster C, Leyser O, Meyerowitz EM (2015) A developmental framework for graft formation and vascular reconnection in *Arabidopsis thaliana*. *Curr Biol* 25: 1306−1318

Pierce NW, Lee JE, Liu X, Sweredoski MJ, Graham RL, Larimore EA, Rome M, Zheng N, Clurman BE, Hess S, Shan SO, Deshaies RJ (2013) Cand1 promotes assembly of new SCF complexes through dynamic exchange of F box proteins. *Cell* 153: 206−215

del Pozo JC, Dharmasiri S, Hellmann H, Walker L, Gray WM, Estelle M (2002) AXR1-ECR1-dependent conjugation of RUB1 to the *Arabidopsis* Cullin AtCUL1 is required for auxin response. *Plant Cell* 14: 421−433

Prigge MJ, Greenham K, Zhang Y, Santner A, Castillejo C, Mutka AM, O'Malley RC, Ecker JR, Kunkel BN, Estelle M (2016) The *Arabidopsis* auxin receptor F-box proteins AFB4 and AFB5 are required for response to the synthetic auxin picloram. *G3 (Bethesda)* 6: 1383−1390

Salehin M, Bagchi R, Estelle M (2015) SCFTIR1/AFB-based auxin perception: mechanism and role in plant growth and development. *Plant Cell* 27: 9−19

Schwechheimer C, Serino G, Callis J, Crosby WL, Lyapina S, Deshaies RJ, Gray WM, Estelle M, Deng XW (2001) Interactions of the COP9 signalosome with the E3 ubiquitin ligase SCFTIRI in mediating auxin response. *Science* 292: 1379−1382

Schwechheimer C, Willige BC (2009) Shedding light on gibberellic acid signalling. *Curr Opin Plant Biol* 12: 57−62

Shang B, Xu C, Zhang X, Cao H, Xin W, Hu Y (2016) Very-long-chain fatty acids restrict regeneration capacity by confining pericycle competence for callus formation in *Arabidopsis*. *Proc Natl Acad Sci USA* 113: 5101−5106

Stuttmann J, Lechner E, Guérois R, Parker JE, Nussaume L, Genschik P, Noël LD (2009a) COP9 signalosome- and 26S proteasome-dependent regulation of SCFTIR1 accumulation in *Arabidopsis*. *J Biol Chem* 284: 7920−7930

Stuttmann J, Parker JE, Noël LD (2009b) Novel aspects of COP9 signalosome functions revealed through analysis of hypomorphic csn mutants. *Plant Signal Behav* 4: 896−898

Tan X, Calderon-Villalobos LI, Sharon M, Zheng C, Robinson CV, Estelle M, Zheng N (2007) Mechanism of auxin perception by the TIR1 ubiquitin ligase. *Nature* 446: 640−645

Tron AE, Arai T, Duda DM, Kuwabara H, Olszewski JL, Fujiwara Y, Bahamon BN, Signoretti S, Schulman BA, DeCaprio JA (2012) The glomuvenous malformation protein Glomulin binds Rbx1 and regulates cullin RING ligase-mediated turnover of Fbw7. *Mol Cell* 46: 67−78

Vierstra RD (2009) The ubiquitin-26S proteasome system at the nexus of plant biology. *Nat Rev Mol Cell Biol* 10: 385−397

Vittal V, Stewart MD, Brzovic PS, Klevit RE (2015) Regulating the regulators: recent revelations in the control of E3 ubiquitin ligases. *J Biol Chem* 290: 21244−21251

Voiniciuc C, Dean GH, Griffiths JS, Kirchsteiger K, Hwang YT, Gillett A, Dow G, Western TL, Estelle M, Haughn GW (2013) Flying saucer1 is a transmembrane RING E3 ubiquitin ligase that regulates the degree of pectin methyl esterification in *Arabidopsis* seed mucilage. *Plant Cell* 25: 944−959

Walker L, Estelle M (1998) Molecular mechanisms of auxin action. *Curr Opin Plant Biol* 1: 434−439

Willige BC, Ghosh S, Nill C, Zourelidou M, Dohmann EM, Maier A, Schwechheimer C (2007) The DELLA domain of GA INSENSITIVE mediates the interaction with the GA INSENSITIVE DWARF1A gibberellin receptor of Arabidopsis. *Plant Cell* 19: 1209−1220

Winkler M, Niemeyer M, Hellmuth A, Janitza P, Christ G, Samodelov SL, Wilde V, Majovsky P, Trujillo M, Zurbriggen MD, Hoehenwarter W, Quint M, Calderón Villalobos LIA (2017) Variation in auxin sensing guides AUX/IAA transcriptional repressor ubiquitylation and destruction. *Nat Commun* 8: 15706

Winter D, Vinegar B, Nahal H, Ammar R, Wilson GV, Provart NJ (2007) An "Electronic Fluorescent Pictograph" browser for exploring and analyzing large-scale biological data sets. *PLoS One* 2: e718

Wu S, Zhu W, Nhan T, Toth JI, Petroski MD, Wolf DA (2013) CAND1 controls *in vivo* dynamics of the cullin 1-RING ubiquitin ligase repertoire. *Nat Commun* 4: 1642

Xu L, Liu F, Lechner E, Genschik P, Crosby WL, Ma H, Peng W, Huang D, Xie D (2002) The SCF(COI1) ubiquitin-ligase complexes are required for jasmonate response in *Arabidopsis*. *Plant Cell* 14: 1919−1935

Yanai O, Shani E, Dolezal K, Tarkowski P, Sablowski R, Sandberg G, Samach A, Ori N (2005) *Arabidopsis* KNOXI proteins activate cytokinin biosynthesis. *Curr Biol* 15: 1566–1571

Yu H, Zhang Y, Moss BL, Bargmann BO, Wang R, Prigge M, Nemhauser JL, Estelle M (2015) Untethering the TIR1 auxin receptor from the SCF complex increases its stability and inhibits auxin response. *Nat Plants* 1: pii: 14030

Zemla A, Thomas Y, Kedziora S, Knebel A, Wood NT, Rabut G, Kurz T (2013) CSN- and CAND1-dependent remodelling of the budding yeast SCF complex. *Nat Commun* 4: 1641

Zheng N, Zhou Q, Wang Z, Wei W (2016) Recent advances in SCF ubiquitin ligase complex: clinical implications. *Biochim Biophys Acta* 1866: 12–22